Atmos. Chem. Phys., 25, 14865–14877, 2025 https://doi.org/10.5194/acp-25-14865-2025 © Author(s) 2025. This work is distributed under the Creative Commons Attribution 4.0 License.





Widespread stratospheric intrusion influence on summer ozone pollution over China revealed by multi-site ozonesonde and validated EAC4 reanalysis

Zhiheng Liao¹, Jinqiang Zhang², Meng Gao³, and Zhiqiang Ma¹

¹Institute of Urban Meteorology, China Meteorological Administration, Beijing, China
²State Key Laboratory of Atmospheric Environment and Extreme Meteorology, Institute of Atmospheric Physics, Chinese Academy of Sciences, Beijing, China
³Department of Geography, Hong Kong Baptist University, Hong Kong SAR, China

Correspondence: Zhiqiang Ma (zqma@ium.cn)

Received: 2 January 2025 – Discussion started: 31 March 2025 Revised: 16 June 2025 – Accepted: 14 August 2025 – Published: 5 November 2025

Abstract. Understanding stratospheric intrusion (SI) is crucial for elucidating atmospheric complexities and improving strategies to mitigate surface ozone (O₃) pollution. This study investigates a deep trough-induced SI event in China from 10 to 13 June 2013, based on ozonesondes from Beijing, Changchun, and Hong Kong, and validated O₃ reanalysis products. Ozonesondes from Beijing indicated notable upper-level secondary O₃ peaks (> 400 ppbv) since 11 June. Tropospheric sub-high O₃ layers were observed in Changchun on 12 June (> 120 ppbv) and Hong Kong on 13 June (> 80 ppbv). Nationwide surface measurements recorded severe O₃ pollution (> 100 ppbv) from western plateaus to eastern plains over China. Together, these observations suggest a widespread influence of stratospheric O₃ intrusion. Further, the ozonesonde-validated EAC4 reanalysis reproduced the fine-scale SI structure (O₃-rich "tongue"), in turn well explaining the secondary O₃ peaks and sub-high O₃ layers in ozonesonde observations. The O₃-rich "tongue" swept through the Tibetan Plateau on 10 June, triggering extreme O_3 pollution with a stratospheric contribution up to 30 ppbv (> 30 %). With the trough's eastward movement, the O₃-rich "tongue" penetrated into the lower troposphere of eastern China, and then entrained into the surface layer, exacerbating surface O₃ pollution occurred in eastern China on 13 June, with a stratospheric O₃ contribution of 3–15 ppbv (2 %–10 %). This research underscores the importance of multi-site ozonesondes in understanding stratospheric O₃ intrusions and the potential of the publicly available EAC4 reanalysis in multiyear SI analyses.

1 Introduction

Surface ozone (O₃) poses significant risks to public health and ecosystem productivity due to its strong oxidative properties (Monks et al., 2015). While O₃ in the lower atmosphere is predominantly produced through photochemical reactions, stratospheric intrusions (SIs) – the process where O₃-rich air masses from the stratosphere descend to the lower troposphere – can also increase surface O₃ concentrations in certain regions (Akritidis et al., 2018; Škerlak et al., 2019; Dreessen, 2019). The natural SI processes complicate efforts to manage and reduce anthropogenic O₃ pollution (Zhao et

al., 2025). Therefore, understanding how SI affects surface O_3 is crucial for improving strategies to mitigate O_3 pollution.

SI is a key component of extratropical weather processes, and detecting SI events and their influence on tropospheric chemistry has been a major scientific concern across Europe (Appenzeller and Davies, 1992; Stohl et al., 2003; Akritidis et al., 2018), North America (Hocking et al., 2007; Lin et al., 2016; Wang et al., 2020b), East Asia (Lin et al., 2021; Liu et al., 2024; Chen et al., 2024), and other extratropical regions (Zhang et al., 2024). Numerous evidence has shown that surface O₃ concentrations can episodically rise during the SI

events (Cristofanelli et al., 2010; Langford et al., 2012; Yates et al., 2013; Lin et al., 2015; Dreessen, 2019; Ou-Yang et al., 2022; Chen et al., 2023; Chen et al., 2024). In previous studies, balloon-based ozonesondes generally served as a key tool for identifying the SI events since it provides complete O₃ profiles up to approximately 35 km. However, the detailed structure of stratospheric O₃ intrusion into the surface layer remains poorly understood due to limited ozonesonde measurements at both temporal and spatial scales (Chen et al., 2011; Zhao et al., 2021; Hong et al., 2024). Consequently, the SI contribution to surface O₃ has long been a topic of much debate over the past few decades (Stohl et al., 2003; Yang et al., 2022; Zheng et al., 2024). Up to now, much of the understanding of SI and its contribution to surface O₃ pollution comes from satellite observations (Li et al., 2015; Zhang et al., 2022; Jaeglé et al., 2017), atmospheric reanalysis (Chen et al., 2023; Knowland et al., 2017; Bartusek et al., 2023; Akritidis et al., 2018), and model simulations (Wang et al., 2020a; Zhao et al., 2021; Zhang et al., 2022; Chang et al., 2023; Hong et al., 2024; Luo et al., 2024; Zhao et al., 2024; Zhu et al., 2024; Škerlak et al., 2019). Due to a common dearth of validation against with ozonesonde measurements, large uncertainties existed in the abovementioned studies. On the other hand, there are some studies that try to quantify stratospheric influences using ground-based chemical tracers, e.g., the ratio of O₃ to CO (O₃/CO) (Ma et al., 2014; Chen et al., 2024), cosmogenic sulfur (35S) (Lin et al., 2016, 2021), and the ratio of cosmogenic beryllium-10 to beryllium-7 (¹⁰Be/⁷Be) (Jordan et al., 2003; Liu et al., 2024). Their results also have embedded uncertainties because little is known about the SI structure aloft from the ground-based measurements alone (Zheng et al., 2024). Opposite conclusions were even drawn from different chemical tracers. For example, a study using ³⁵S as chemical tracer (Lin et al., 2021) revealed a west-high-east-low SI contribution over China, whereas a study using O₃/CO ratio as tracer (Chen et al., 2024) suggested an inverse distribution of SI contribution. The lack of consensus led to significant cognitive confusion, emphasizing the urgent need for direct ozonesonde observations to refine the fundamental understanding of stratospheric O₃ intrusion and its contribution to surface O₃ pollution.

This study focuses on a typical SI event associated with a high-level trough observed over China during 10–13 June 2013. During this event, severe surface O₃ pollution successively occurred in the high-elevation Tibetan Plateau and low-altitude eastern China. To explore the potential linkage between the SI process and O₃ pollution, we combined multi-site consecutive ozonesondes, ground-based O₃ measurements, satellite O₃ products, and atmospheric O₃ reanalysis. Through detailed analysis of multi-source data in this SI event, this study aims to (1) characterize the spatial and temporal behavior of high-level trough-induced stratospheric O₃ intrusion, (2) quantify the SI contribution to surface O₃

pollution and (3) elucidate the underlying dynamical mechanisms.

2 Datasets

2.1 Ozonesonde observation

In China, ozonesondes, along with radiosondes, were routinely launched weekly in Beijing (39.80° N, 116.47° E) and Hong Kong (22.31° N, 114.17° E). During June 2013, an intensive ozonesonde launch experiment was held in Beijing and Changchun (43.90° N, 125.20° E), with consecutive launches from 10 to 13 June. The details of the intensive experiment can be found in Zhang et al. (2013). These sondes (including the routine ozonesonde in Hong Kong) were launched around 13:30 China Standard Time, providing high-resolution profiles of O₃ partial pressure, atmospheric pressure, temperature, and humidity from the surface up to approximately 35 km (Zhang et al., 2021; Liao et al., 2024). For this study, data from nine ozonesonde observations were analyzed to examine stratospheric O₃ intrusion during 10-13 June 2013, including 4 consecutive days in Beijing and Changchun, and a single launch on 13 June in Hong Kong. By comparing the sonde-based surface O₃ concentrations with ground-based O₃ measurements (Fig. 3b), we demonstrated good accuracy of these ozonesonde observations (R = 0.981 and MAB = 3.2 ppbv).

2.2 Atmospheric reanalysis data

ERA5, the fifth-generation ECMWF (European Centre for Medium-Range Weather Forecasts) global reanalysis, offers a comprehensive dataset at a spatial resolution of $0.25^{\circ} \times 0.25^{\circ}$ and a temporal resolution of 1 h for climate and weather analysis (Hersbach et al., 2020). It integrates model data with observations using four-dimensional variational assimilation in ECMWF's Integrated Forecast System (IFS). This study utilized ERA5 data, including geopotential height, potential vorticity, and wind fields, to describe the synoptic conditions during the stratospheric intrusion event.

EAC4 (ECMWF Atmospheric Composition Reanalysis 4) represents the fourth generation of ECMWF's atmospheric composition reanalysis, with a spatial resolution of 0.75° × 0.75° and a temporal resolution of 3 h (Inness et al., 2019). EAC4 assimilates data from various satellite sources, including total column O₃ from the Ozone Monitoring Instrument and Global Ozone Monitoring Experiment-2 on MetOp satellites, profile data from the Microwave Limb Sounder, and partial columns from Solar Backscatter Ultra-Violet and Ozone Mapping and Profiler Suite. Note that surface O₃ measurements and ozonesonde O₃ profile data in China are not assimilated into the EAC4 reanalysis. The IFS used in EAC4 incorporates an extended version of the Carbon Bond 2005 chemical mechanism, which includes 126 tropospheric reactions. The emission datasets are com-

posed of anthropogenic emissions from the MACCity inventory (Granier et al., 2011), biogenic emissions from the MEGAN2.1 model (Guenther et al., 2006), and biomass burning emissions from the Global Fire Assimilation System (Kaiser et al., 2012). Apart from O₃, the stratospheric O₃ tracer (O₃S, O₃ originating from the stratosphere) is also provided in the EAC4 reanalysis. This study employed both O₃ and O₃S to characterize the three-dimensional structure of stratospheric O₃ intrusion.

2.3 Auxiliary data

Additional data sources included ground-based O₃ measurements from the China National Air Quality Monitoring Network and the Hong Kong Environmental Protection Department, satellite cloud images from the Moderate Resolution Imaging Spectroradiometer (MODIS), satellite O₃ products from the Atmospheric Infrared Sounder (AIRS) (Aumann et al., 2003), and atmospheric O₃ reanalysis from the Modern-Era Retrospective Analysis for Research and Applications, Version 2 (MERRA2) (Gelaro et al., 2017). According to previous studies (Jaeglé et al., 2017; Knowland et al., 2017; Zhang et al., 2022), we used satellite O₃ retrieved from AIRS Level 3 product, which has a spatial resolution of $1^{\circ} \times 1^{\circ}$. In contrast, the MERRA2 reanalysis has a spatial resolution of $0.5^{\circ} \times 0.625^{\circ}$. Both AIRS and MERRA2 O₃ products served as alternative references to EAC4 O₃ reanalysis to provide a large-scale view of horizontal and vertical O₃ structures during the SI event. Hourly surface O₃ concentrations from 77 cities in China (including Hong Kong) were used to assess nationwide O₃ pollution during the stratospheric intrusion event.

3 Results

3.1 Ozonesonde evidence of stratospheric O₃ intrusion

Figure 1 illustrates the evolution of the upper-level trough event from 10 to 13 June 2013. On 10 June, the upper-level trough extended from the Mongolian Plateau towards the Tibetan Plateau. By 11 June, the trough had moved eastward and deepened into a "V-shaped" structure between 90 and 120°E, causing an extremely distorted westerly jet and strong northerlies at the western flank of the trough. On this day, the emerged 1.5 PVU potential vorticity contours at 400 hPa provide convincing evidence for a deep stratospheric intrusion. On 12 June, the "V-shaped" trough persisted at 200 hPa. By 13 June, the upper-level trough had weakened to be a shallow structure over the North China Plain (NCP). Three-dimensional dynamics associated with upper-level troughs involves stratospheric dry intrusion (SDI) and warm conveyor belt (WCB) airstreams (Browning and Roberts, 1994; Browning, 1997). The SDI originates in the lower stratosphere on the cold side of the trough (west of the trough axis) and descends behind the cold front, while the WCB originates in the warm sector of the trough (east of the trough axis), ascending rapidly to the middle and upper troposphere. During this event, these contrasting airstreams led to significantly different weather conditions at the two sides of the trough, with cloudy weather in the WCB zone (east) and clear weather in the SDI zone (west). There appeared an obvious transition from cloudy to clear weather in the eastern China with the eastward movement of upper-level trough. On 13 June, China, excluding the northeast and eastern coastal regions, experienced clear weather.

Previous ozonesonde-based observational studies (Lemoine, 2004; Hwang et al., 2007; Chen et al., 2011; Ojha et al., 2017) revealed that a secondary O₃ peak in a height range between 9 and 16 km (i.e., near the tropopause) is a characteristic O₃-profile structure when SI occurs and triggers tropopause folding. The continuous and multi-site ozonesondes in this study provided a unique opportunity to characterize stratospheric O₃ intrusion linked to an upperlevel trough from an observational perspective (Fig. 2). On 10 June, before the trough arrived, Beijing was influenced by WCB airstreams, showing high relative humidity (> 60 %) in the upper troposphere. By 11 June, Beijing was near the trough axis, and the O₃-rich SDI airstream began to affect the upper atmosphere, creating a secondary O₃ peak (~ 400 ppbv at 9.5 km height) just above the rapidly descended thermal tropopause (which dropped from 10.5 km on 10 June to 8.2 km on 11 June). Besides, the cold dry air of the SDI led to a quick drop in relative humidity from 70 % on 10 June to below 25 % on 11 June in the upper troposphere of Beijing. On 12 and 13 June, the secondary O₃ peaks continued to be observed over Beijing, with peak concentrations rising to 650 ppbv by 13 June, but the altitude of these peaks gradually increased up to 13.6 km by 13 June with the increase in thermal tropopause height. Unlike that in Beijing, the sonde-based O₃ profiles in Changchun showed secondary O₃ peak only in 13 June, when upper-level trough moved eastward to affect Changchun. However, sub-high O₃ layer (> 120 ppbv) appeared in the middle troposphere (4.2–8.1 km height, the shaded light gray in Fig. 2) in advance on 12 June, accompanied by extremely low relative humidity. This sub-high O₃ layer is likely the transport result of pre-intruded O₃ from stratosphere over Beijing or its surroundings. Similar sub-high O_3 layer (> 80 ppbv) also occurred in the lower troposphere (3.5-6.0 km height, the shaded light gray in Fig. 2) of Hong Kong (a subtropical city) on 13 June. These high-O₃ and low-humidity air masses in the troposphere reflect obvious stratospheric origin, suggesting a widespread SI influence from extratropics to subtropics during this deep trough event.

Three-dimensional structure of stratospheric O₃ intrusion

The multi-site ozonesonde observations only provide a snapshot of stratospheric O_3 intrusion. To further visualize the

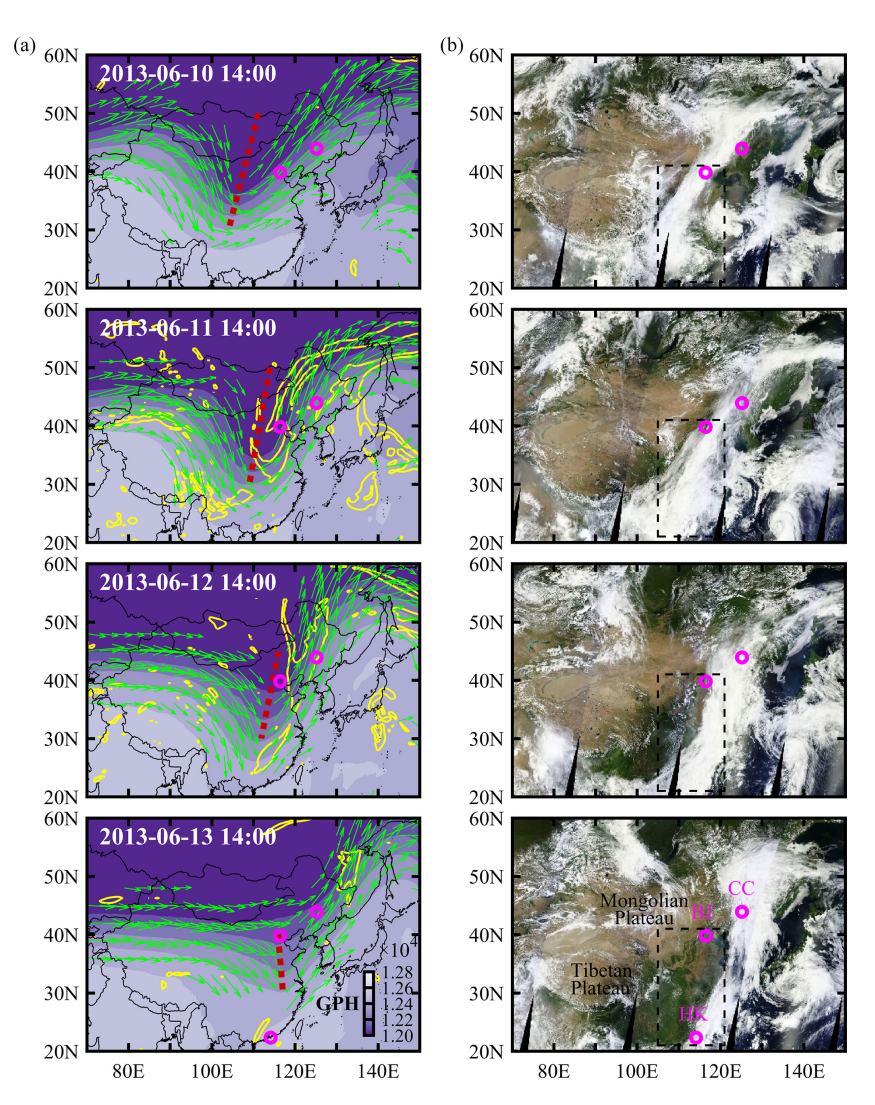


Figure 1. (a) Horizontal distribution of geopotential height (shading, gpm), and wind direction of jet stream in excess of 20 m s⁻¹ (arrows) at 200 hPa, and potential vorticity of 1.5 PVU (blue contours) at 400 hPa. (b) MODIS satellite cloud images with the dashed box marking eastern China (21–41° N, 105–121° E). Red dot lines in panel (a) denote the axis of the upper-level trough at 200 hPa. Magenta circles in panels (a) and (b) mark the available ozonesondes at different sites (BJ: Beijing, CC: Changchun, and HK: Hong Kong) on different days.

three-dimensional structure, we introduced the commonly used O₃ products, including AIRS satellite observation, MERRA2 and EAC4 reanalysis (Li et al., 2015; Knowland et al., 2017; Akritidis et al., 2018). These three large-scale O₃ products were firstly validated against our ozonesonde observations. As shown in Fig. 2, AIRS satellite observation missed the upper-level secondary O₃ peaks and the boundary layer O₃ enhancements. MERRA2 reanalysis captured the secondary O₃ peaks but still showed large negative biases to the observed boundary layer O₃ enhancements. In contrast, EAC4 reanalysis reproduced well the major features of the O₃ vertical distribution, including upper-level secondary O₃ peaks and boundary layer O₃ enhancements. Particularly, EAC4 exactly captured the SI-induced sub-high O₃ layers in the middle troposphere of Changchun (on 12 June) and the

lower troposphere of Hong Kong (on 13 June). This qualitative comparison suggests that EAC4 had a powerful ability to reproduce both the SI dynamics and boundary layer photochemical processes. The scatter comparison with quantitative statistics in Fig. 3a further demonstrates that EAC4 O_3 reanalysis had the strongest correlation (R = 0.947), the lowest mean absolute bias (MAB = 19.1 ppbv), the lowest root mean square error (RMSE = 36.9 ppbv), and the largest index of agreement (IOA = 0.985) with the ozonesonde observation. This sonde-based validation (Fig. 3a), along with validation against with nationwide surface O_3 observations (Figs. 3b and 5a), provides us enough confidence in adopting EAC4 reanalysis to explore the three-dimensional structure of trough-induced stratospheric O_3 intrusion.

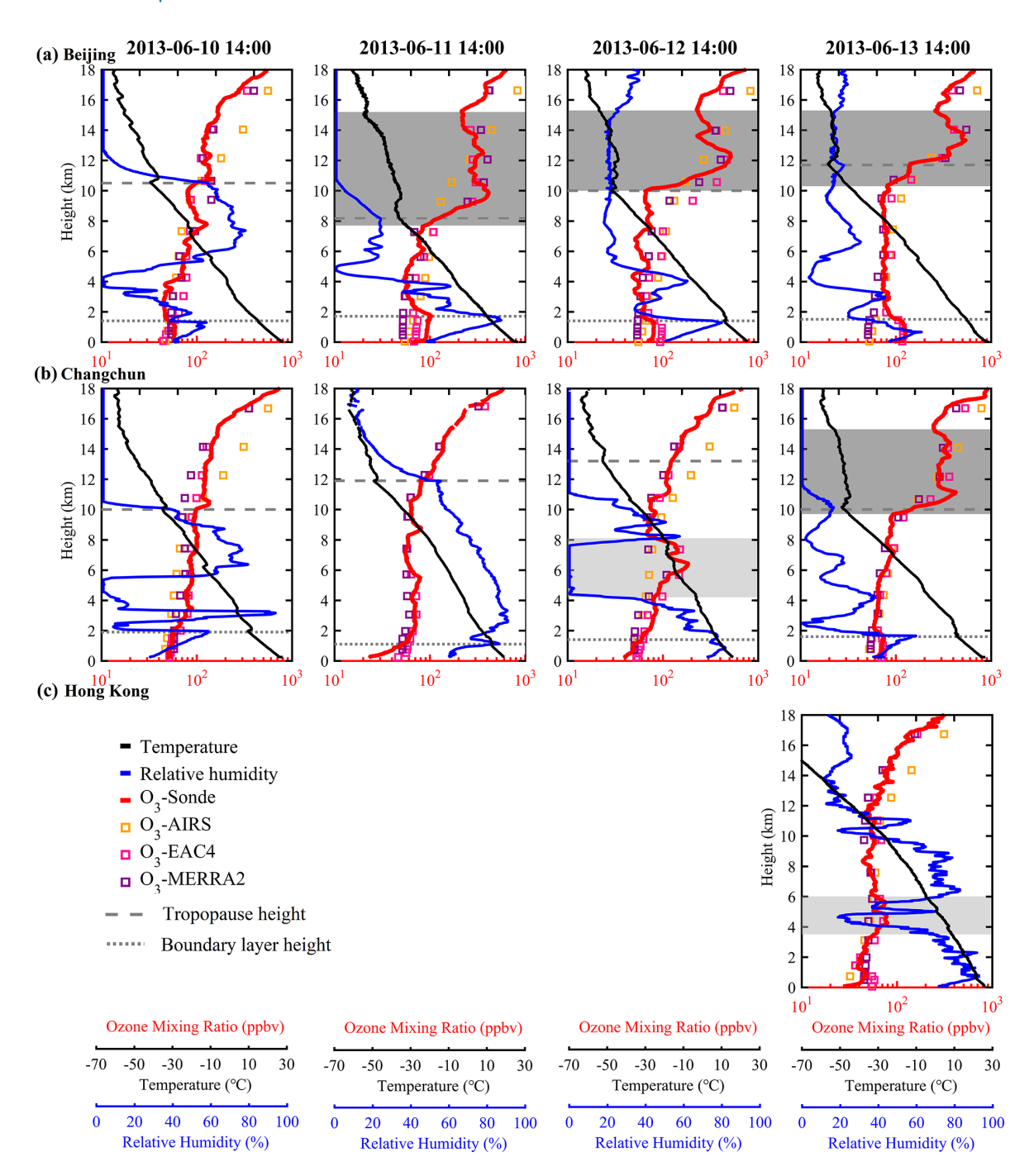


Figure 2. O₃ vertical distribution over (a) Beijing, (b) Changchun, and (c) Hong Kong derived from ozonesonde and other data sources (including AIRS satellite observation, EAC4 and MERRA2 reanalysis) during 10–13 June 2013. Black and blue lines denote the sonde-based temperature and relative humidity profiles, respectively. Gray dashed lines represent the thermal tropopause height, and gray dot lines indicate the boundary layer top height. Upper-level secondary O₃ peaks are shaded heavy gray, and SI-induced O₃-rich layer in the troposphere is shaded light gray.

Figure 4 illustrates the EAC4-based three-dimensional structure of upper-level trough-induced stratospheric O_3 intrusions over China. High O_3 concentrations at $200\,hPa$ aligned with the trough location, extending southwestward (10 June) and southward (11–13 June) along the trough

axis, which explained the upper-level secondary O_3 peaks over Beijing since 11 June and over Changchun on 13 June well (Fig. 2a and b). The stratospheric intrusions developed into elongated (about 2000 km) and slender (about 2000 km) streamers with elevated O_3 concentrations exceed-

ing 150 ppbv (referred to as SDI-induced O₃-rich belts) at 400 hPa. On the east of the SDI streamers, the WCB streamers were parallel with anomalously low O₃ concentrations (referred to as WCB-related O₃-poor belts). On 12 June, the SDI-induced O₃-rich belt stretched to northeastern China, explaining the observed sub-high O₃ layer in the middle troposphere of Changchun (Fig. 2b). In the lower troposphere (700 hPa), O₃-rich air masses appeared over subtropical southern China on 11 June, the strongest SI day, indicating the southern edge of stratospheric O₃ intrusion. These lower-tropospheric O₃-rich air masses persisted on subsequent days and were able to be captured exactly by Hong Kong's ozonesonde on 13 June (Fig. 2c). From 11 to 13 June, there was a significant northeastward transport and dispersion of O₃-rich filament due to the strengthening southwesterly winds in the lower troposphere of eastern China. Through vertical and horizontal transport, lowertropospheric O₃ concentrations increased by approximately 20 ppbv across eastern China, consistent with the 18 ppbv O₃ increase observed at 2–6 km height over Beijing, indicating widespread enhancement of lower-tropospheric O₃ background due to stratospheric O₃ intrusion and accumulation.

Compared with total O₃, O₃S provides a more direct view of stratospheric intrusion (Fig. 4b). The three-dimensional O₃S structure depicts the upper-level trough-induced stratospheric O₃ intrusion as a sheet-like lowering of the O₃S-rich layer along the western flank of the trough and an O₃Srich tongue extending southward and westward from the trough base. These features aligned well with the typical structure of extratropical stratospheric intrusion associated with tropopause folding (Bithell et al., 1999; Hocking et al., 2007). On 10 June, stratospheric O₃ intrusion directly hit the Tibetan Plateau, triggering extremely high surface O₃ concentrations. From 11 to 13 June, the O₃S-rich tongue progressed eastward into eastern China with the trough's eastward movement. Unlike that on the Tibetan Plateau, the O₃Srich tongue in eastern China was blocked in the lower free troposphere and did not further intrude the surface layer. This result agreed well with the observed sub-high O₃ layer at 3.5-6.0 km height over Hong Kong (Fig. 2c), suggestive of no direct stratospheric O₃ intrusion to the surface in the low-elevation eastern China. Nevertheless, these O₃-rich stratospheric air masses can be further transported into atmospheric boundary layer via convective mixing pathway, contributing to boundary layer O₃ increase. In this process, their stratospheric characteristics (high O₃, low humidity) tend to be lost due to strong turbulence mixing, eventually becoming unrecognizable in atmospheric boundary layer. Interestingly, another stratospheric intrusion induced by severe tropical storm (name: "Yagi") over the northwestern Pacific provided a parallel reference (Fig. 4b). Compared with the tropical storm-induced stratospheric O₃ instruction, the upper-level trough-induced intrusion descended to a relatively lower altitude, causing widespread O₃S signals in the atmospheric boundary layer over eastern China. Note that apart from the trough- and storm-induced SI, a secondary SI emerged in the upwind of upper-level trough on 12 June likely driven by peripheral compensatory flows. This secondary SI led to elevated O_3 concentrations over the Mongolian Plateau (Fig. 4a). However, they were not further transported into eastern China.

3.3 Stratospheric intrusion contribution to surface O₃ pollution

Figure 5a presents the spatial distribution of surface O₃ concentrations derived from ground-based measurements and EAC4 reanalysis during the SI event. The EAC4based surface O₃ reanalysis agreed well with nationwide ground-based observations (R = 0.697, MAB = 12.4 ppbv, RMSE = 23.5 ppbv, and IOA = 0.961, Fig. 3b), again confirming the reliability of the EAC4 reanalysis as in the previous validation with ozonesondes. On 10 June, the Tibetan Plateau experienced high O₃ concentrations near or exceeding 80 ppbv, with observed O₃ in Lhasa reaching up to 100 ppbv at 14:00 BJT. In contrast, eastern China exhibited low O₃ concentrations (< 40 ppbv) due to cloudy and rainy weather on this day. From 10 to 13 June, surface O₃ concentrations decreased day by day on the Tibetan Plateau, while they increased from west to east in eastern China. By 13 June, eastern China suffered severe O₃ pollution, with observed O₃ concentrations exceeding 100 ppbv in most of the NCP cities. From 10 to 13 June, the continuous stratospheric dry intrusion led to a weather transition from cloudy to cloudless in eastern China (Fig. 1b), enhancing photochemical O₃ production due to the abundance of O_3 precursors over there. On the other hand, strong solar radiation in cloudless weather promoted the development of thermal convection, facilitating the mixing of pre-intruded O₃-rich stratospheric air from the lower free troposphere into the surface layer. These two mechanisms combined to trigger severe O₃ pollution in eastern China on 13 June. The continue ozonesondes in Beijing provide convincing evidence for these two mechanisms. Returning to Fig. 2a, boundary layer O₃ concentrations in Beijing increased significantly from 57.8 ppbv on 10 June to 120.6 ppbv on 13 June. Considering the sharp O₃ gradient in the interface between the atmospheric boundary layer and the lower free troposphere, the dramatic increase in boundary layer O₃ can be primarily attributed to photochemical production (Liao et al., 2024). However, the concurrent rise in O₃ concentrations in the lower free troposphere (an 18 ppbv O₃ increase at 2–6 km height from 10 to 13 June) indicated that stratospheric O₃ intrusion contributed to elevating lowertropospheric O₃ background, ultimately exacerbating boundary layer O₃ pollution.

To quantify the contribution of stratospheric intrusion to surface O_3 pollution, Fig. 5b illustrates the spatial distribution of EAC4-based surface O_3S concentrations during the SI event, and Fig. 5c shows the contribution fraction (CF) of O_3S in surface O_3 concentrations (CF = $100 \% \times O_3S/O_3$).

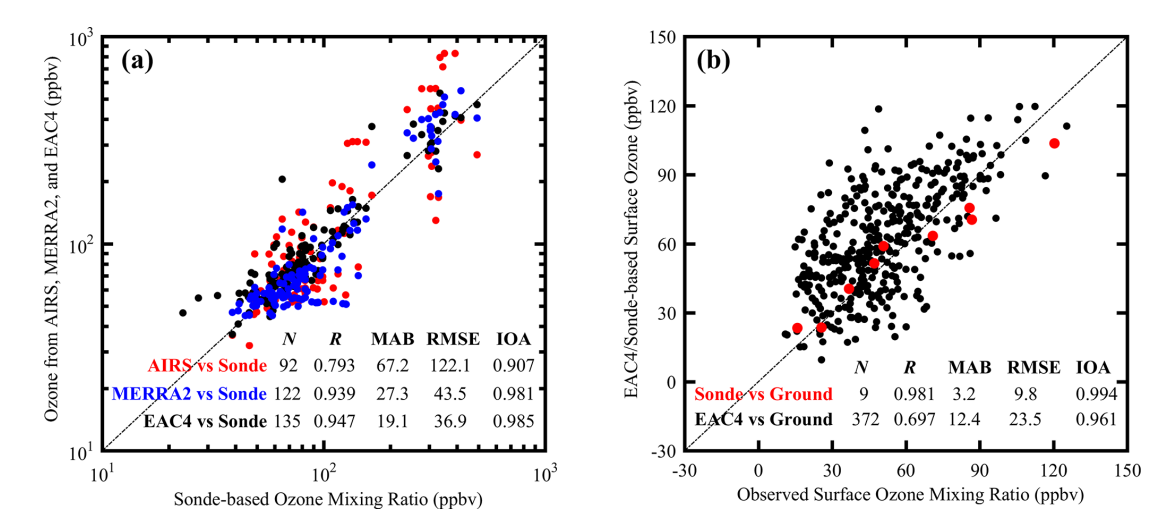


Figure 3. (a) Validation of AIRS, MERRA2, and EAC4 O_3 products with nine ozonesonde observations from Beijing, Changchun, and Hong Kong. (b) Validation of EAC4/sonde-based surface O_3 concentrations with ground-based O_3 observations. In panel (a), AIRS, MERRA2, and EAC4 O_3 data were spatially interpolated to the location of ozonesonde stations. In panel (b), ground-based O_3 observations across 466 sites in 76 cities were resampled to EAC4 grid $(0.75^{\circ} \times 0.75^{\circ})$ for comparison with EAC4-based surface ozone reanalysis; ground-based O_3 observations at three neighboring sites (Tiantan site in Beijing, Daishan Park site in Changchun, and Sham Shui Po site in Hong Kong) were used for comparison with sonde-based surface ozone concentrations. N, R, MAB, RMSE, and IOA denote the number of statistic samples, correlation coefficient, mean absolute bias, root mean square error, and index of agreement, respectively.

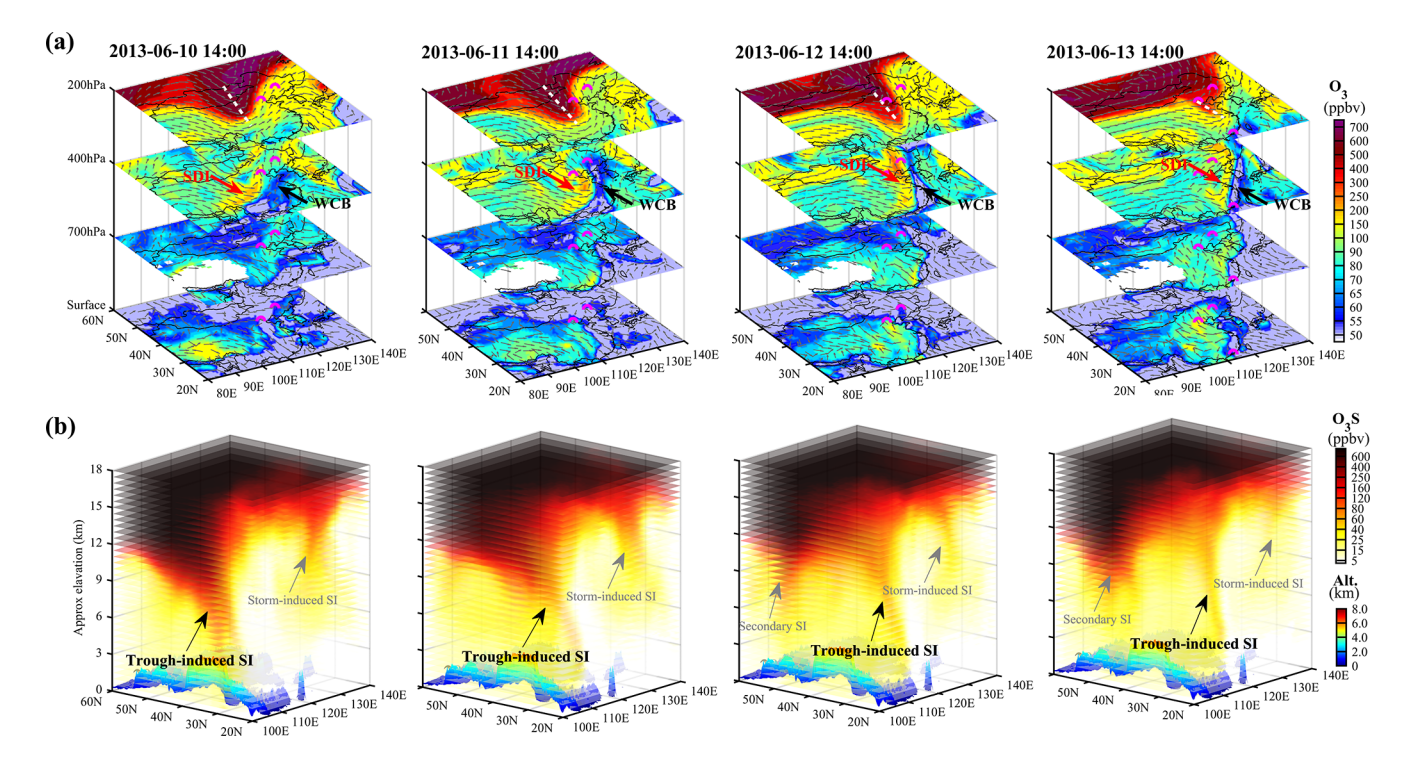


Figure 4. (a) Spatial distribution of O₃ concentrations in 200, 400, 700 hPa, and surface layer. (b) Three-dimensional structure of O₃S concentrations. In panel (a), white dashed lines mark the trough axis at 200 hPa, and magenta half-circles mark the locations of ozonesondes at different sites (Beijing, Changchun and Hong Kong) on different days.

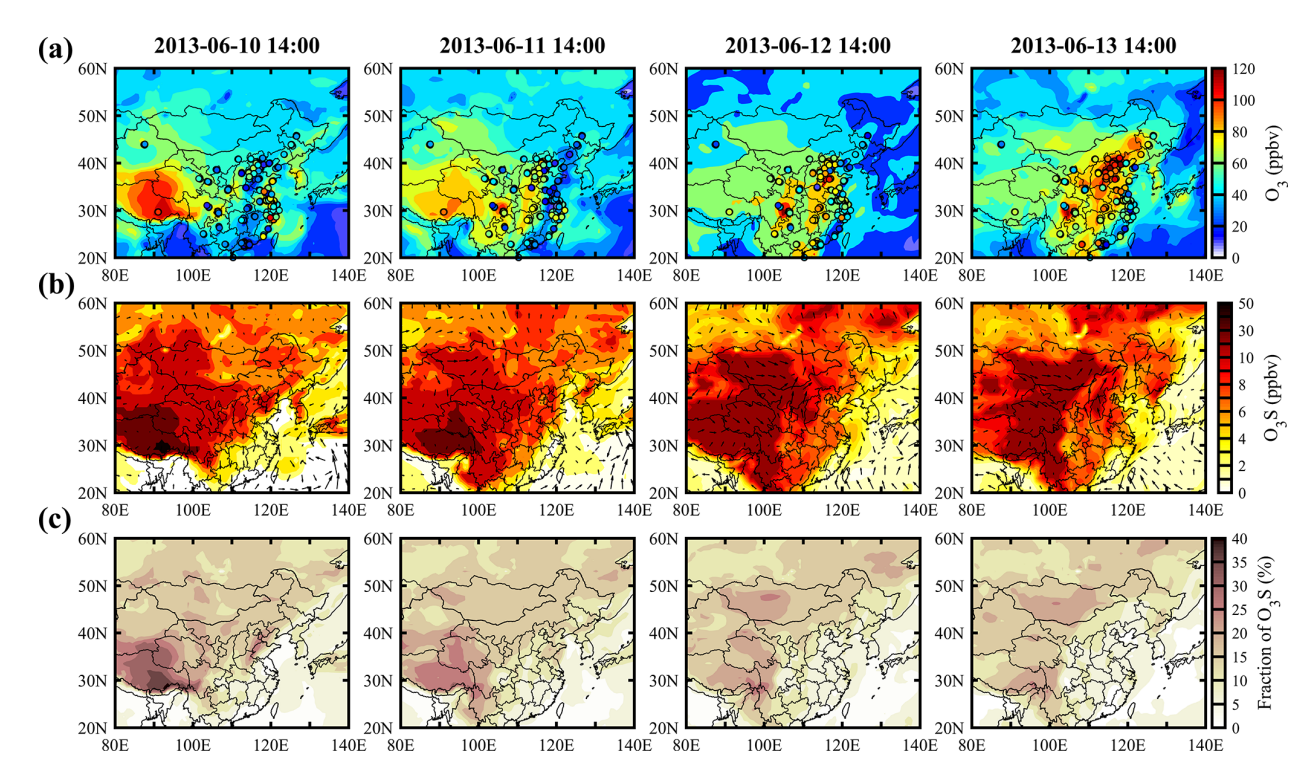


Figure 5. (a) Surface spatial distribution of the total O_3 concentration derived from ground-based measurement (dots) and EAC4 reanalysis (shading). (b) Surface spatial distribution of O_3S concentration derived from EAC4 reanalysis. (c) Spatial distribution of O_3S fraction in surface O_3 concentration calculated from EAC4 reanalysis.

The high-elevation Tibetan Plateau received a high concentration O₃ from stratospheric intrusion, particularly on 10 June, when the upper-level trough was oriented northeastsouthwest towards the Tibetan Plateau. On this day, surface O₃S concentration exceeded 30 ppbv (up to 48.5 ppbv) on the Tibetan Plateau, contributing to over $30\,\%$ of the surface O₃ concentration (up to 44.7 %). Subsequent days saw a gradual decrease in O₃S over the Tibetan Plateau. On 12 and 13 June, significant O₃S hotspots (> 20 ppbv) appeared in the Mongolian Plateau. In conjunction with the three-dimensional O₃S structure (Fig. 4b), the elevated O₃S concentrations in the Mongolian Plateau can be attributed to the emerged secondary SI on 12 June rather than initial trough-induced SI. It seems that the elevated O₃S in the Mongolian Plateau had no influences on surface O3 over eastern China considering its downwind location in the lower troposphere. Nonetheless, eastern China was affected not only by the "fresh" stratospheric air in the eastward movement O₃S-rich tongue (via convective mixing), but also by the pre-intruded "aged" stratospheric air from the Tibetan Plateau (via eastward transport). Due to continuous accumulation, region-averaged O₃S concentrations increased approximately 1.0 ppbv in eastern China from 10 to 13 June, whereas their fraction in surface O₃ decreased from 11.8 % to 8.3 % as local O₃ photochemical production accelerated. On 13 June, surface O₃S concentrations in eastern China ranged from 3 to 15 ppbv, accounting for 2 %-10 % of surface O₃

concentrations. Particularly in the highly polluted NCP region, O_3S contributed approximately 10% of surface O_3 , reflecting a non-negligible role of stratospheric O_3 intrusion in exacerbating surface O_3 pollution.

4 Conclusions and discussion

This study reveals that the upper-level trough-induced stratospheric O₃ intrusion over China did not occur as a localscale vertical descent from the stratosphere to the lower troposphere just at the mid-latitude location where tropopause folding occurs; instead, it involved a long-range transport from mid-latitude tropopause folding zone (e.g., Beijing) to lower-latitude areas (e.g., Hong Kong), featuring an O₃-rich "tongue" structure with upper-level secondary O₃ peak at the base of tongue (e.g., over Beijing) and lower-tropospheric sub-high O₃ layer at the tip of tongue (e.g., over Hong Kong). The O₃-rich "tongue" swept through the high-elevation Tibetan Plateau when the upper-level trough extended towards this highland region at its initial stage, triggering extreme surface O₃ pollution. With the eastward movement of upperlevel trough, the O₃-rich "tongue" penetrated into the lower troposphere of low-elevation eastern China. Over there, the intruded O₃-rich stratospheric air masses in the lower troposphere, including the "fresh" stratospheric air vertically transported from O₃-rich "tongue" and the "aged" strato-

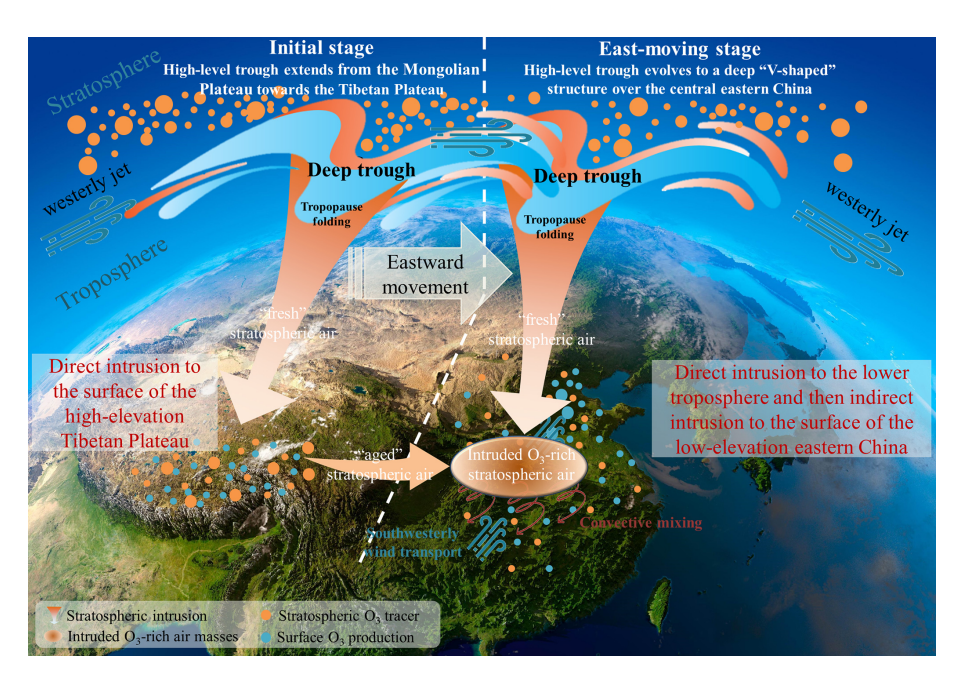


Figure 6. Schematic illustration of upper-level trough-induced stratospheric O₃ intrusion influence on surface O₃ pollution over China.

spheric air horizontally transported from the Tibetan Plateau, were then entrained into the atmospheric boundary layer via lower-tropospheric dynamic processes (e.g. convective mixing). At the same time, the strengthening lower-tropospheric southwesterly winds with the eastward movement of upper-level trough gradually participated to transport these O₃-rich stratospheric air back to the mid-latitudes, ultimately exacerbating surface O₃ pollution in the NCP region (e.g., Beijing). While several SI events have been reported in China (Chang et al., 2023; Hong et al., 2024; Li et al., 2015; Luo et al., 2024; Wang et al., 2020a; Zhang et al., 2022; Zhao et al., 2024), this trough-induced SI episode may be the first event of its widespread impact and refined structure documented (Fig. 6).

The quantitative stratospheric intrusion contributions derived from the validated EAC4 reanalysis are generally consistent with previous model results in China. In the lowelevation eastern China, surface O₃S concentrations were previously estimated to be in the range of 5–20 ppbv during the SI events (Wang et al., 2020a; Zhang et al., 2022; Chang et al., 2023). Our EAC4-based estimation agreed well with this range, reflecting the typical magnitude of SI contribution in the low-elevation eastern China. As for the high-elevation Tibetan Plateau, a case-based model study (Škerlak et al., 2019) revealed that stratospheric tracer concentrations at the surface reach peak values of 20% of the imposed stratospheric value, and a month-based model study (Yin et al., 2023) suggested that 36.5 % of surface O₃ in the hotspot of the southern Tibetan Plateau was contributed by stratospheric O₃ intrusion. Our EAC4-based estimation was comparable to these fractional contributions, corroborating the potential of SI to significantly influence surface O₃ concentrations in this highland region. Besides, ground-based chemical tracer method had been developed to quantify the stratospheric intrusion contribution over China. While Chen et al. (2024) identified the nationwide SI-induced O₃ enhancement as a west-low-east-high spatial distribution pattern based on surface O₃ and CO observations, Lin et al. (2021) determined a west-high-east-low spatial distribution pattern of SI-induced O₃ contribution based on ground-based cosmogenic ³⁵S observations at the Himalayas and beyond. Our result appears to support the latter, which conforms to the common knowledge that the highland regions are more susceptible to stratospheric intrusion because of their proximity to the stratosphere (Škerlak et al., 2019; Wang et al., 2020b; Lin et al., 2021).

To the best of our knowledge, this study is the first to utilize continuous and multi-site ozonesondes to investigate stratospheric O₃ intrusion. While we acknowledge that a single case study may not be fully representative, it effectively demonstrates the value of continuous and multi-site ozonesonde measurements in enhancing our understanding of stratospheric O₃ intrusion phenomena. On the other hand, these continuous and multi-site ozonesondes provide a valuable and unique benchmark for examining the capacity of those commonly used O₃ products (including AIRS satellite observation, MERRA2 and EAC4 O3 reanalysis) in characterizing stratospheric O₃ intrusion. Previous study indicated that MERRA2 can be used in scientific studies to identify SIs by both atmospheric dynamics and composition (Knowland et al., 2017). Here, we demonstrate that EAC4, a publicly available dataset from the European Centre for MediumRange Weather Forecasts, performs better than MERRA2 in quantitatively characterizing stratospheric O₃ intrusion via comparative evaluation. Moreover, in contrast to MERRA2, EAC4 simulates full O₃ chemistry in the troposphere (an extended version of the Carbon Bond 2005 (CB05) chemical mechanism), allowing us to determine the influence of stratospheric O₃ on surface concentrations separate from photochemically produced O₃. Therefore, this is a proof opening the door to detailed multiyear analyses of stratospheric O₃ intrusion and their quantitative contribution to surface O₃ over China and worldwide based on the publicly available EAC4 O₃ reanalysis.

Data availability. All of the used data, excluding the ozonesonde in Beijing and Changchun, are open source. ERA5 atmospheric data are available from the Copernicus Climate Change Service (C3S) Climate Data Store accessible at https://cds.climate.copernicus.eu/ (last access: 2 January 2025). EAC4 O₃ reanalysis data were obtained from the Copernicus Atmospheric Monitoring Service Data Store accessible at https://ads.atmosphere.copernicus.eu/ (last access: 2 January 2025). The MODIS true color images are available from the NASA Earth Observations (NEO) at https://neo.gsfc. nasa.gov/ (last access: 2 January 2025). The AIRS and MERRA2 O₃ products were obtained from Goddard Earth Sciences Data and Information Services Center accessible at https://disc.gsfc.nasa. gov/ (last access: 2 January 2025). The ozonesonde data in Hong Kong were obtained from World Ozone and Ultraviolet Radiation Data Centre accessible at https://woudc.org/ (last access: 2 January 2025). The ozonesonde data for Beijing and Changchun are available from the first author upon reasonable request (zhliao@ium.cn).

Author contributions. ZL conceived the original idea, analyzed the data, and wrote the first version of the manuscript. JZ designed intensive ozonesonde experiments in Beijing and Changchun. ZM supervised the research project. All of the authors discussed the results and commented on the manuscript.

Competing interests. The contact author has declared that none of the authors has any competing interests.

Disclaimer. Publisher's note: Copernicus Publications remains neutral with regard to jurisdictional claims made in the text, published maps, institutional affiliations, or any other geographical representation in this paper. While Copernicus Publications makes every effort to include appropriate place names, the final responsibility lies with the authors. Also, please note that this paper has not received English language copy-editing. Views expressed in the text are those of the authors and do not necessarily reflect the views of the publisher.

Acknowledgements. We acknowledge the Copernicus Climate Change Service Climate Data Store, the Copernicus Atmospheric Monitoring Service Data Store, NASA Earth Observations, God-

dard Earth Sciences Data and Information Services Center, and the World Ozone and Ultraviolet Radiation Data Centre for their data support.

Financial support. This research has been supported by the National Natural Science Foundation of China (grant nos. 42405115, 42293321 and 42207115).

Review statement. This paper was edited by William Ward and reviewed by three anonymous referees.

References

- Akritidis, D., Katragkou, E., Zanis, P., Pytharoulis, I., Melas, D., Flemming, J., Inness, A., Clark, H., Plu, M., and Eskes, H.: A deep stratosphere-to-troposphere ozone transport event over Europe simulated in CAMS global and regional forecast systems: analysis and evaluation, Atmos. Chem. Phys., 18, 15515–15534, https://doi.org/10.5194/acp-18-15515-2018, 2018.
- Appenzeller, C. and Davies, H. C.: Structure of stratospheric intrusions into the troposphere, Nature, 358, 570–572, https://doi.org/10.1038/358570a0, 1992.
- Aumann, H. H., Chahine, M. T., Gautier, C., Goldberg, M. D., Kalnay, E., McMillin, L. M., Revercomb, H., Rosenkranz, P. W., Smith, W. L., Staelin, D. H., Strow, L. L., and Susskind, J.: AIRS/AMSU/HSB on the Aqua mission: design, science objectives, data products, and processing systems, IEEE Transactions on Geoscience and Remote Sensing, 41, 253–264, https://doi.org/10.1109/TGRS.2002.808356, 2003.
- Bartusek, S., Wu, Y. T., Ting, M. F., Zheng, C., Fiore, A., Sprenger, M., and Flemming, J.: Higher-Resolution Tropopause Folding Accounts for More Stratospheric Ozone Intrusions, Geophys. Res. Lett., 50, e2022GL101690, https://doi.org/10.1029/2022GL101690, 2023.
- Bithell, M., Gray, L. J., and Cox, B. D.: A Three-Dimensional View of the Evolution of Midlatitude Stratospheric Intrusions, Journal of the Atmospheric Sciences, 56, 673–688, https://doi.org/10.1175/1520-0469(1999)056<0673:ATDVOT>2.0.CO;2, 1999.
- Browning, K. A.: The dry intrusion perspective of extra-tropical cyclone development, Meteorological Applications, 4, 317–324, https://doi.org/10.1017/S1350482797000613, 1997.
- Browning, K. A. and Roberts, N. M.: Structure of a frontal cyclone, Q. J. Roy. Meteor. Soc., 120, 1535–1557, https://doi.org/10.1002/qj.49712052006, 1994.
- Chang, F. Y., Li, J. D., Li, N., and Liao, H.: Stratospheric intrusion may aggravate widespread ozone pollution through both vertical and horizontal advections in eastern China during summer, Front. Env. Sci.-Switz., 10, 1115746, https://doi.org/10.3389/Fenvs.2022.1115746, 2023.
- Chen, X. L., Ma, Y. M., Kelder, H., Su, Z., and Yang, K.: On the behaviour of the tropopause folding events over the Tibetan Plateau, Atmos. Chem. Phys., 11, 5113–5122, https://doi.org/10.5194/acp-11-5113-2011, 2011.
- Chen, Z., Liu, J., Qie, X., Cheng, X., Yang, M., Shu, L., and Zang, Z.: Stratospheric influence on surface ozone pollution in China,

- Nat. Commun., 15, 4064, https://doi.org/10.1038/s41467-024-48406-x, 2024.
- Chen, Z. X., Liu, J. E., Cheng, X. G., Yang, M. M., and Shu, L.: Stratospheric influences on surface ozone increase during the COVID-19 lockdown over northern China, Npj Clim. Atmos. Sci., 6, 76, https://doi.org/10.1038/S41612-023-00406-2, 2023.
- Cristofanelli, P., Bracci, A., Sprenger, M., Marinoni, A., Bonafè, U., Calzolari, F., Duchi, R., Laj, P., Pichon, J. M., Roccato, F., Venzac, H., Vuillermoz, E., and Bonasoni, P.: Tropospheric ozone variations at the Nepal Climate Observatory-Pyramid (Himalayas, 5079 m a.s.l.) and influence of deep stratospheric intrusion events, Atmos. Chem. Phys., 10, 6537–6549, https://doi.org/10.5194/acp-10-6537-2010, 2010.
- Dreessen, J.: A Sea Level Stratospheric Ozone Intrusion Event Induced within a Thunderstorm Gust Front, B. Am. Meteorol. Soc., 100, 1259–1275, https://doi.org/10.1175/Bams-D-18-0113.1, 2019.
- Gelaro, R., McCarty, W., Suárez, M. J., Todling, R., Molod, A., Takacs, L., Randles, C. A., Darmenov, A., Bosilovich, M. G., Reichle, R., Wargan, K., Coy, L., Cullather, R., Draper, C., Akella, S., Buchard, V., Conaty, A., da Silva, A. M., Gu, W., Kim, G.-K., Koster, R., Lucchesi, R., Merkova, D., Nielsen, J. E., Partyka, G., Pawson, S., Putman, W., Rienecker, M., Schubert, S. D., Sienkiewicz, M., and Zhao, B.: The Modern-Era Retrospective Analysis for Research and Applications, Version 2 (MERRA-2), Journal of Climate, 30, 5419–5454, https://doi.org/10.1175/JCLI-D-16-0758.1, 2017.
- Granier, C., Bessagnet, B., Bond, T., D'Angiola, A., Denier van der Gon, H., Frost, G. J., Heil, A., Kaiser, J. W., Kinne, S., Klimont, Z., Kloster, S., Lamarque, J.-F., Liousse, C., Masui, T., Meleux, F., Mieville, A., Ohara, T., Raut, J.-C., Riahi, K., Schultz, M. G., Smith, S. J., Thompson, A., van Aardenne, J., van der Werf, G. R., and van Vuuren, D. P.: Evolution of anthropogenic and biomass burning emissions of air pollutants at global and regional scales during the 1980–2010 period, Climatic Change, 109, 163, https://doi.org/10.1007/s10584-011-0154-1, 2011.
- Guenther, A., Karl, T., Harley, P., Wiedinmyer, C., Palmer, P. I., and Geron, C.: Estimates of global terrestrial isoprene emissions using MEGAN (Model of Emissions of Gases and Aerosols from Nature), Atmos. Chem. Phys., 6, 3181–3210, https://doi.org/10.5194/acp-6-3181-2006, 2006.
- Hersbach, H., Bell, B., Berrisford, P., Hirahara, S., Horányi, A., Muñoz-Sabater, J., Nicolas, J., Peubey, C., Radu, R., Schepers, D., Simmons, A., Soci, C., Abdalla, S., Abellan, X., Balsamo, G., Bechtold, P., Biavati, G., Bidlot, J., Bonavita, M., De Chiara, G., Dahlgren, P., Dee, D., Diamantakis, M., Dragani, R., Flemming, J., Forbes, R., Fuentes, M., Geer, A., Haimberger, L., Healy, S., Hogan, R. J., Hólm, E., Janisková, M., Keeley, S., Laloyaux, P., Lopez, P., Lupu, C., Radnoti, G., de Rosnay, P., Rozum, I., Vamborg, F., Villaume, S., and Thépaut, J. N.: The ERA5 global reanalysis, Q. J. Roy. Meteor. Soc., 146, 1999–2049, https://doi.org/10.1002/qj.3803, 2020.
- Hocking, W. K., Carey-Smith, T., Tarasick, D. W., Argall, P. S., Strong, K., Rochon, Y., Zawadzki, I., and Taylor, P. A.: Detection of stratospheric ozone intrusions by windprofiler radars, Nature, 450, 281–284, https://doi.org/10.1038/nature06312, 2007.
- Hong, J., Wang, H., Wang, W., Zhu, J., Deng, H., and Wang, H.: Impacts of stratosphere-to-troposphere transport on tropospheric ozone in southeastern China: insights from

- ozonesonde observations, Environ. Res. Lett., 19, 064068, https://doi.org/10.1088/1748-9326/ad4ef9, 2024.
- Hwang, S. H., Kim, J., and Cho, G. R.: Observation of secondary ozone peaks near the tropopause over the Korean peninsula associated with stratosphere-troposphere exchange, J. Geophys. Res.-Atmos., 112, D16305, https://doi.org/10.1029/2006jd007978, 2007.
- Inness, A., Ades, M., Agustí-Panareda, A., Barré, J., Benedictow, A., Blechschmidt, A.-M., Dominguez, J. J., Engelen, R., Eskes, H., Flemming, J., Huijnen, V., Jones, L., Kipling, Z., Massart, S., Parrington, M., Peuch, V.-H., Razinger, M., Remy, S., Schulz, M., and Suttie, M.: The CAMS reanalysis of atmospheric composition, Atmos. Chem. Phys., 19, 3515–3556, https://doi.org/10.5194/acp-19-3515-2019, 2019.
- Jaeglé, L., Wood, R., and Wargan, K.: Multiyear Composite View of Ozone Enhancements and Stratosphere-to-Troposphere Transport in Dry Intrusions of Northern Hemisphere Extratropical Cyclones, Journal of Geophysical Research: Atmospheres, 122, 13436–13457, https://doi.org/10.1002/2017JD027656, 2017.
- Jordan, C. E., Dibb, J. E., and Finkel, R. C.: ¹⁰Be/⁷Be tracer of atmospheric transport and stratosphere-troposphere exchange, Journal of Geophysical Research: Atmospheres, 108, https://doi.org/10.1029/2002JD002395, 2003.
- Kaiser, J. W., Heil, A., Andreae, M. O., Benedetti, A., Chubarova, N., Jones, L., Morcrette, J.-J., Razinger, M., Schultz, M. G., Suttie, M., and van der Werf, G. R.: Biomass burning emissions estimated with a global fire assimilation system based on observed fire radiative power, Biogeosciences, 9, 527–554, https://doi.org/10.5194/bg-9-527-2012, 2012.
- Knowland, K. E., Ott, L. E., Duncan, B. N., and Wargan, K.: Strato-spheric Intrusion-Influenced Ozone Air Quality Exceedances Investigated in the NASA MERRA-2 Reanalysis, Geophys. Res. Lett., 44, 10691–10701, https://doi.org/10.1002/2017GL074532, 2017.
- Langford, A. O., Brioude, J., Cooper, O. R., Senff, C. J., Alvarez, R. J., Hardesty, R. M., Johnson, B. J., and Oltmans, S. J.: Stratospheric influence on surface ozone in the Los Angeles area during late spring and early summer of 2010, J. Geophys. Res.-Atmos., 117, D00v06, https://doi.org/10.1029/2011jd016766, 2012.
- Lemoine, R.: Secondary maxima in ozone profiles, Atmos. Chem. Phys., 4, 1085–1096, https://doi.org/10.5194/acp-4-1085-2004, 2004.
- Li, D., Bian, J. C., and Fan, Q. J.: A deep stratospheric intrusion associated with an intense cut-off low event over East Asia, Sci. China Earth Sci., 58, 116–128, https://doi.org/10.1007/s11430-014-4977-2, 2015.
- Liao, Z., Gao, M., Zhang, J., Sun, J., Quan, J., Jia, X., Pan, Y., and Fan, S.: Mixing-layer-height-referenced ozone vertical distribution in the lower troposphere of Chinese megacities: stratification, classification, and meteorological and photochemical mechanisms, Atmos. Chem. Phys., 24, 3541–3557, https://doi.org/10.5194/acp-24-3541-2024, 2024.
- Lin, M., Su, L., Shaheen, R., Fung, J. C. H., and Thiemens, M. H.: Detection of deep stratospheric intrusions by cosmogenic ³⁵S, P. Natl. Acad. Sci. USA, 113, 11131–11136, https://doi.org/10.1073/pnas.1609919113, 2016.
- Lin, M., Wang, K., Kang, S., Li, Y., Fan, Z., and Thiemens, M. H.: Isotopic signatures of stratospheric air at

- the Himalayas and beyond, Sci. Bull., 66, 323–326, https://doi.org/10.1016/j.scib.2020.11.005, 2021.
- Lin, M. Y., Fiore, A. M., Horowitz, L. W., Langford, A. O., Oltmans, S. J., Tarasick, D., and Rieder, H. E.: Climate variability modulates western US ozone air quality in spring via deep stratospheric intrusions, Nat. Commun., 6, 7105, https://doi.org/10.1038/Ncomms8105, 2015.
- Liu, X., Fu, Y., Zhang, L., Li, H., Burr, G. S., Bi, Y., and Zhao, G.: Deep stratospheric intrusion events in China revealed on the ground by cosmogenic ¹⁰Be/⁷Be, Communications Earth & Environment, 5, 553, https://doi.org/10.1038/s43247-024-01727-7, 2024.
- Luo, Y., Zhao, T., Meng, K., Hu, J., Yang, Q., Bai, Y., Yang, K., Fu, W., Tan, C., Zhang, Y., Zhang, Y., and Li, Z.: A mechanism of stratospheric O₃ intrusion into the atmospheric environment: a case study of the North China Plain, Atmos. Chem. Phys., 24, 7013–7026, https://doi.org/10.5194/acp-24-7013-2024, 2024.
- Ma, J., Lin, W. L., Zheng, X. D., Xu, X. B., Li, Z., and Yang, L. L.: Influence of air mass downward transport on the variability of surface ozone at Xianggelila Regional Atmosphere Background Station, southwest China, Atmos. Chem. Phys., 14, 5311–5325, https://doi.org/10.5194/acp-14-5311-2014, 2014.
- Monks, P. S., Archibald, A. T., Colette, A., Cooper, O., Coyle, M., Derwent, R., Fowler, D., Granier, C., Law, K. S., Mills, G. E., Stevenson, D. S., Tarasova, O., Thouret, V., von Schneidemesser, E., Sommariva, R., Wild, O., and Williams, M. L.: Tropospheric ozone and its precursors from the urban to the global scale from air quality to short-lived climate forcer, Atmos. Chem. Phys., 15, 8889–8973, https://doi.org/10.5194/acp-15-8889-2015, 2015.
- Ojha, N., Pozzer, A., Akritidis, D., and Lelieveld, J.: Secondary ozone peaks in the troposphere over the Himalayas, Atmos. Chem. Phys., 17, 6743–6757, https://doi.org/10.5194/acp-17-6743-2017, 2017.
- Ou-Yang, C. F., Babu, S. R., Lee, J. R., Yen, M. C., Griffith, S. M., Lin, C. C., Chang, S. C., and Lin, N. H.: Detection of stratospheric intrusion events and their role in ozone enhancement at a mountain background site in sub-tropical East Asia, Atmos. Environ., 268, 118779, https://doi.org/10.1016/j.atmosenv.2021.118779, 2022.
- Škerlak, B., Pfahl, S., Sprenger, M., and Wernli, H.: A numerical process study on the rapid transport of stratospheric air down to the surface over western North America and the Tibetan Plateau, Atmos. Chem. Phys., 19, 6535–6549, https://doi.org/10.5194/acp-19-6535-2019, 2019.
- Stohl, A., Bonasoni, P., Cristofanelli, P., Collins, W., Feichter, J., Frank, A., Forster, C., Gerasopoulos, E., Gäggeler, H., James, P., Kentarchos, T., Kromp-Kolb, H., Krüger, B., Land, C., Meloen, J., Papayannis, A., Priller, A., Seibert, P., Sprenger, M., Roelofs, G. J., Scheel, H. E., Schnabel, C., Siegmund, P., Tobler, L., Trickl, T., Wernli, H., Wirth, V., Zanis, P., and Zerefos, C.: Stratosphere-troposphere exchange: A review, and what we have learned from STACCATO, J. Geophys. Res.-Atmos., 108, 8516, https://doi.org/10.1029/2002jd002490, 2003.
- Wang, H. Y., Wang, W., Huang, X., and Ding, A. J.: Impacts of stratosphere-to-troposphere-transport on summertime surface ozone over eastern China, Sci. Bull., 65, 276–279, https://doi.org/10.1016/j.scib.2019.11.017, 2020a.
- Wang, X. Y., Wu, Y. T., Randel, W., and Tilmes, S.: Stratospheric contribution to the summertime high surface ozone events over

- the western united states, Environ. Res. Lett., 15, 1040a6, https://doi.org/10.1088/1748-9326/abba53, 2020b.
- Yang, J., Wang, K., Lin, M., Yin, X., and Kang, S.: Not biomass burning but stratospheric intrusion dominating tropospheric ozone over the Tibetan Plateau, P. Natl. Acad. Sci. USA, 119, e2211002119, https://doi.org/10.1073/pnas.2211002119, 2022.
- Yates, E. L., Iraci, L. T., Roby, M. C., Pierce, R. B., Johnson, M. S., Reddy, P. J., Tadić, J. M., Loewenstein, M., and Gore, W.: Airborne observations and modeling of springtime stratosphere-to-troposphere transport over California, Atmos. Chem. Phys., 13, 12481–12494, https://doi.org/10.5194/acp-13-12481-2013, 2013.
- Yin, X., Rupakheti, D., Zhang, G., Luo, J., Kang, S., de Foy, B., Yang, J., Ji, Z., Cong, Z., Rupakheti, M., Li, P., Hu, Y., and Zhang, Q.: Surface ozone over the Tibetan Plateau controlled by stratospheric intrusion, Atmos. Chem. Phys., 23, 10137–10143, https://doi.org/10.5194/acp-23-10137-2023, 2023.
- Zhang, J.-q., Xuan, Y., Xia, X.-A., Liu, M., Yan, X.-I., Pang, L., Bai, Z.-X., and Wang, X.: Performance Evaluation of a Self-Developed Ozonesonde and Its Application in an Intensive Observational Campaign, Atmospheric and Oceanic Science Letters, 7, 175–179, 2013.
- Zhang, J., Gong, X., Crosbie, E., Diskin, G., Froyd, K., Hall, S., Kupc, A., Moore, R., Peischl, J., Rollins, A., Schwarz, J., Shook, M., Thompson, C., Ullmann, K., Williamson, C., Wisthaler, A., Xu, L., Ziemba, L., Brock, C. A., and Wang, J.: Stratospheric air intrusions promote global-scale new particle formation, Science, 385, 210–216, https://doi.org/10.1126/science.adn2961, 2024.
- Zhang, J. Q., Li, D., Bian, J. C., Xuan, Y. J., Chen, H. B., Bai, Z. X., Wan, X. W., Zheng, X. D., Xia, X. G., and Lu, D. R.: Long-term ozone variability in the vertical structure and integrated column over the North China Plain: results based on ozonesonde and Dobson measurements during 2001–2019, Environ. Res. Lett., 16, 074053, https://doi.org/10.1088/1748-9326/Ac109f, 2021.
- Zhang, Y. J., Li, J., Yang, W. Y., Du, H. Y., Tang, X., Ye, Q., Wang, Z. X., Sun, Y. L., Pan, X. L., Zhu, L. L., and Wang, Z. F.: Influences of stratospheric intrusions to high summer surface ozone over a heavily industrialized region in northern China, Environ. Res. Lett., 17, 094023, https://doi.org/10.1088/1748-9326/Ac8b24, 2022.
- Zhao, K., Chen, Y., Lian, P., Li, W., Yang, F., Zhang, X., and Yang, R.: Impact of stratospheric intrusions on surface ozone enhancement in Hong Kong in the lower troposphere: Implications for ozone control strategy, Atmos. Environ., 329, 120539, https://doi.org/10.1016/j.atmosenv.2024.120539, 2024.
- Zhao, K., Chen, W., Lian, P., and Xu, D.: Optimizing Ozone Control Strategies for Chinese Megacity Clusters Under the Influence of Stratospheric Intrusion, Journal of Geophysical Research: Atmospheres, 130, e2024JD043112, https://doi.org/10.1029/2024JD043112, 2025.
- Zhao, K. H., Huang, J. P., Wu, Y. H., Yuan, Z. B., Wang, Y. W., Li, Y., Ma, X. D., Liu, X. H., Ma, W., Wang, Y., and Zhang, X. Y.: Impact of Stratospheric Intrusions on Ozone Enhancement in the Lower Troposphere and Implication to Air Quality in Hong Kong and Other South China Regions, J. Geophys. Res.-Atmos., 126, e2020JD033955, https://doi.org/10.1029/2020JD033955, 2021.
- Zheng, X., Yang, W., Sun, Y., Geng, C., Liu, Y., and Xu, X.: Comment on "Transport of substantial stratospheric ozone to the surface by a dying typhoon and shallow convection" by

Chen et al. (2022), Atmos. Chem. Phys., 24, 3759–3768, https://doi.org/10.5194/acp-24-3759-2024, 2024.

Zhu, F., Luo, J., Wang, Z., Jin, H., Zhao, Q., Wang, Z., Luo, F., and Gu, M.: The Impact of Stratosphere-to-Troposphere Transport Associated with the Northeast China Cold Vortex on Surface Ozone Concentrations in Eastern China, Journal of Applied Meteorology and Climatology, https://doi.org/10.1175/JAMC-D-24-0027.1, 2024.